Proceedings of the Institute of Acoustics

EVALUATION OF OBJECT SPECULAR REFLECTION IN ACOUSTICAL IMAGING, WITH SPECIAL EMPHASIS ON SYNTHETIC APERTURE SYSTEMS

M. Granara Whitehead Alenia Sistemi Subacquei, Via Puccini 2, Genoa, Italy
M. Palmese Department of Biophysical and Electronic Engineering(DIBE), University of Genoa, Italy
A.Trucco Department of Biophysical and Electronic Engineering(DIBE), University of Genoa, Italy

1 INTRODUCTION

It is widely recognized that one of the major problems affecting the coherent imaging field (both acoustical or electromagnetic) is represented by the specular reflection produced by the structures having surfaces that are poorly rough with respect to the adopted wavelength. Generally, man-made objects show this characteristic. Due to this effect, the images often show little, very bright spots instead of the expected shape of the involved objects [1,2,3].

In this paper, the mentioned phenomenon is analytically analysed for two different imaging approaches: active systems that insonify the scene from a given spatial point and using a physical aperture to collect the echoes, and active systems that exploit a synthetic aperture concept, insonifying the scene and collecting the related echo from many points along the same spatial aperture. Although more complex solutions are used in real systems that adopt a physical aperture or a synthetic aperture, the two simplified schemes investigated in this paper are representative of the different philosophies.

The analysis is carried out by considering the effects that are due to the envelope detection performed in an acoustic imaging system. Despite the linearity of beamforming [3,4], envelope extraction is a non-linear operation that destroys phase information and introduces, at the output of the beamformer, some non-linear terms that might cause a strong degradation of the process. As widely discussed in [5], the non-linear contribution produced by the envelope detection dramatically contributes to the specular reflection, by adding large positive values to the beam intensity when the object is parallel to the array and in front of it.

In [5], the importance of the non-linear contribution and the related specular effects have been evaluated by a beam-pattern-like mathematical formulation. Here, such a formulation is recalled and further developed to investigate and compare the cases of physical aperture and synthetic aperture. The analysis allows to justify the reduction of the specular reflection occurring when the synthetic aperture imaging is performed, in accordance with the results obtained by the experimental practice. In addition, the role in reducing the specular reflection of the non-linear contribution due to the envelope extraction operation is clarified.

2 PROBLEM DEFINITION

For a simple data definition, we assume that the scene to be observed, i.e., the smooth surface of a continuous objects, is composed of a set of ideal punctiform scatterers, and that K spherical waves arrive at the array, one for each reflecting point forming the scene. We also assume that the k-th wave has an arrival angle α_k, comes from a distance Rk from the coordinate origin, and produces, at the outputs of an hypothetical punctiform omnidirectional receiver placed in the origin of the coordinates, a complex signal $x_k(t)$ [3].

Under a quasi-steady-state hypothesis (i.e., a narrow bandwidth) [3,6], and if the cone that has the vertex in the coordinate origin and that contains the object to be imaged has an angular aperture that is not too wide (i.e., applying the Fresnel approximation for the Green function) [3,7], thanks to the linearity of the coherent focused beamforming, the beam signal at the output of the beamformer, y (t), can be written as follows:

$$y(t) = \sum_{k=1}^{K} y_k(t) \quad (1)$$

$$y_k(t) = CBP_{\theta,R_0}(\alpha_k, R_k) \cdot x_k(t) \quad (2)$$

where $CBP_{\theta,R0}(\alpha_k, Rk)$ is the complex beam pattern dependent on the array characteristics (i.e., number of elements, element spacing, frequency) [3,4] and represents the attenuation applied to the wave incoming from an α_k direction and a Rk distance, provided that the beam signal is steered in the θ direction [4,8] and focused at a distance R0.

As we represent all the signals as time-dependent phasors (i.e., the equivalent low-pass representation for pass-band signals), the envelope detection can be performed through a modulus operation, and the intensity detection through a square modulus operation. We analysed the case in which the beam signal is processed by a square-modulus block, obtaining the intensity z(t) expressed as:

$$z(t) = |y(t)|^2 = \sum_{k=1}^{K} BPP_{\theta,R_0}(\alpha_k, R_k) \cdot |x_k(t)|^2 + \sum_{k=1}^{K} \sum_{l=1, l\neq k}^{K} \mathrm{Re}\left\{ y_k(t) \cdot y_l(t)^* \right\} \quad (3)$$

where * is the complex conjugate operator, Re{·} is the real-part operator, and $CBP_{\theta,R0}(\alpha_k, Rk)$ is the beam power pattern equal to $|CBP_{\theta,R0}(\alpha_k, Rk)|^2$ [3,4].

The first term in the third member of Eq. (3) is a sum of received wave intensities, each of them is weighted by the value of the beam power pattern resulting from its incidence angle and distance of origin. The second term is a mixed term that defines the non-linear effects introduced by the square modulus. In more detail, one can rewrite the real signal z(t) as a sum of three different signals:

$$z(t) = a(t) + b(t) + c(t) \quad (4)$$

$$a(t) = \sum_{k \in MLR} BPP_{\theta,R_0}(\alpha_k, R_k) \cdot |x_k(t)|^2 \quad (5)$$

$$b(t) = \sum_{k \notin MLR} BPP_{\theta,R_0}(\alpha_k, R_k) \cdot |x_k(t)|^2 \quad (6)$$

$$c(t) = \sum_{k=1}^{K} \sum_{l=1, l\neq k}^{K} \mathrm{Re}\left\{ CBP_{\theta,R_0}(\alpha_k, R_k) \cdot CBP_{\theta,R_0}(\alpha_l, R_l)^* \cdot x_k(t) \cdot x_l(t)^* \right\} \quad (7).$$

MLR stands for main lobe region and $k \in$ MLR takes into account all the scene points covered by the main lobe, when the steering angle is θ.

Although the signal b(t) is a spurious signal, both a(t) and b(t) represent two signals that are expected, as they represent linear weighted sums of received wave intensities and have been obtained by splitting the first term in the third member of Eq. (3) into two parts: one is due to the main lobe and the other is due to the side lobes.

Finally, we denoted by c(t) the mixed term due to the non-linearity of the square envelope detection. In the following, we evaluate the importance of the non-linear contribution c(t) as compared with the signals a(t) and b(t), both for the physical and the synthetic aperture schemes.

It is worth noticing that, if the received signals are pulses, then, in general, the longer the overlapping time of the received signals, the greater the importance of the signal c(t). Therefore, to analyse the significance of the non-linear contribution related to the worst condition, we make the assumption that the received pulses are amplitude-modulated and time-overlapped signals, with the same envelope shape and amplitude, but with different constant phases, due to the distances of the related scatterers. Denoting by A(t) the envelope of the received pulses, we can write: $x_k(t) = A(t) \cdot \exp(j\varphi_k)$ and $x_l(t) = A(t) \cdot \exp(j\varphi_l)$, where φ_k and φ_l are the phases of the signals that are backscattered from the k-th and l-th points in a scene, respectively. Substituting $x_k(t)$ and $x_l(t)$ into Eq. (4), we obtain:

$$z(t) = A(t)^2 \cdot \left[\begin{array}{l} \sum_{k \in MLR} BPP_{\theta,R_0}(\alpha_k, R_k) + \sum_{k \notin MLR} BPP_{\theta,R_0}(\alpha_k, R_k) + \\ + \sum_{k=1}^{K} \sum_{l=1, l \neq k}^{K} \mathrm{Re}\left\{ CBP_{\theta,R_0}(\alpha_k, R_k) \cdot CBP_{\theta,R_0}(\alpha_l, R_l)^* \cdot \exp(j\Delta) \right\} \end{array} \right] \quad (8)$$

where Δ is equal to the difference between the phases of the two received signals $x_k(t)$ and $x_l(t)$ (i.e., $\Delta = \varphi_k - \varphi_l$). The three addenda in Eq. (8) do not depend on time any more; therefore, to assess their relative importance [5], it is possible to evaluate the behaviour of the summation arguments.

3 PHYSICAL AND SYNTHETIC APERTURES

In this paper, we consider a linear equispaced array with a Physical Aperture (PA) or a Synthetic Aperture (SA).

In the PA case, the insonification of the whole scene is assumed to be produced by an omnidirectional transducer placed in the coordinate origin and the acoustic image is generated processing the echoes collected by the sensors of the linear array, that is equispaced and centred in the coordinate origin. In this way, a phased array structure is assumed in which the echoes collected and stored after a single insonification of the scene are used by a digital beamformer to compute a fan of beams that scan the angular sector of interest. According to [3], the complex beam pattern can be written as follows:

$$CBP_{\theta,R_0}(\alpha_k, R_k) = \sum_{i=1}^{N} w_i \exp\left\{ j \frac{\omega}{c} \left[p_i(\sin\alpha_k - \sin\theta) + \frac{p_i^2}{2R_0} - \frac{p_i^2}{2R_k} \right] \right\} \quad (9)$$

where *N* is the number of sensors composing the receiving array, *pi* is the coordinate of the *i*-th sensor, *wi* is the apodizing coefficient assigned to the *i*-th sensor, *c* is the sound velocity, and ω is the angular frequency of the carrier.

In the SA case, a single omnidirectional transducer, suited to emit and receive, is moved along a linear spatial aperture, stopping at a set of predetermined positions. At each position, the transducer insonifies the whole scene and collects the related echo. After the entire aperture is scanned, the collected echoes are processed by a digital beamformer to compute a fan of beams that scan the angular sector of interest. As in the PA case, such beams are used to compose the acoustic image. In the described SA scheme, the complex beam pattern in Eq. (9) should be updated by adding a factor 2 in the exponent, as follows:

$$CBP_{\theta,R_0}(\alpha_k, R_k) = \sum_{i=1}^{N} w_i \exp\left\{ j \frac{\omega}{c} 2 \left[p_i(\sin\alpha_k - \sin\theta) + \frac{p_i^2}{2R_0} - \frac{p_i^2}{2R_k} \right] \right\} \quad (10)$$

Obviously, the meaning of *N*, *pi*, and *wi* should be updated as follows: *N* is the number of positions at which the transducer stopped, *pi* is the coordinate of the *i*-th position, and *wi* is the apodizing coefficient assigned to the *i*-th position.

Finally, for both the PA and the SA cases, the phase, φk, of the complex signal $xk(t)$ due to the k-th scatterer can be written as:

$$\varphi_k = \frac{-\omega}{c} 2R_k \,. \qquad (11)$$

Indeed, the differences between the PA and the SA are fully encompassed in the 2 complex beam pattern formulations, whereas the phases of the signals due to the scatterers are the same (despite such scatterers are differently insonified under the 2 considered cases).

4 SIMULATION RESULTS AND DISCUSSION

In order to assess the relevance of the specular behaviour, we assumed that the imaging system uses an array made up of 51 elements, spaced 3 mm each other, in both the PA and the SA cases.

The carrier frequency is of 1 MHz, the sound velocity is assumed to be 1500 m/s, and a Dolph-Chebyschev apodization to achieve a side-lobe level equal to -30 dB is applied. In this way, the overall aperture is of 15 cm and the inter-element space is 2λ (λ being the wavelength).

Concerning the scene, a smooth object can be modelled as a collection of densely packed point scatterers [3,9]. We consider a flat, rectangular object, placed parallel to the array baseline, at a distance of 1 m. The rectangular object is 8 cm large, 2 mm high, and 1850 points are used to simulate it.

A set of 25 beam signals are computed to scan the region from –0.07 rad to 0.07 rad that largely contains the rectangular object, keeping the focalisation distance equal to 1 m. Due to the spatial undersampling, the array beam patterns contain some grating lobes, in both the PA and the SA cases. However, the very limited steering angles and the presence of just one small object inside the scene assure that the grating lobes do not impact at all.

Concerning the PA case, in Fig. 1, the behaviours of the terms *a*, *b*, *c*, and their sum *z* are plotted versus the steering angle. In order to avoid effect due to the random nature of the scatterers' positions, the 4 graphs are the average of 10 different realizations.

The linear term *a*, shown in Fig. 1(a), provides a good image of the rectangular object as it is correctly detected for steering angles between –0.04 and 0.04 rad, in accordance with the scene geometry and the expected angular resolution. Moreover, the object response is quasi-constant inside such an angular interval.

The linear term *b* due to the side lobes, shown in Fig. 1(b), is negligible owing to its very low amplitude.

The mixed term *c*, shown in Fig. 1(c), definitely accounts for the specular effect, as it exhibits a huge peak, that is tight around the steering direction perpendicular to the object surface, i.e., $\theta = 0$ rad.

As expected for the specular effect, and differently from the term *a*, the peak width is not directly related to the angular extension of the object. The latter produces just a small base that is several times lower than the peak. The final image, i.e., the sum of the 3 terms shown in Fig. 1(d), is sharply dominated by the term *c*, having the terms *a* and *b* a negligible impact, and reflects the scene geometry only partially. Essentially, the image shows a bright spot close the direction perpendicular to the object surface.

Concerning the SA case, in Fig. 2, the behaviours of the terms *a*, *b*, *c*, and their sum *z* are plotted versus the steering angle. Also in this case, the 4 graphs are the average of 10 different realizations to mitigate the random placement of the discrete scatterers.

It is important to recall that, for the scatterers placed at a distance equal to the focalisation distance (i.e., when $R_k = R_0$), the beam pattern of the SA case is exactly the same of the PA case, provided that the spatial aperture is doubled. The angular resolution is improved accordingly.

The linear term *a*, shown in Fig. 2(a), provides a good image of the rectangular object as it is correctly detected for steering angles between –0.04 and 0.04 rad, accordingly with the scene geometry. The image edges are more precise than in the PA case, as in the SA case the angular resolution is improved by a factor 2. Moreover, the object response is quasi-constant inside the angular interval in which the object is comprised.

As the main lobe width is decreased with respect to the PA case, the amplitude of the term *a* decreases, whereas the amplitude of the term *b* increases. Nevertheless, the linear term *b*, shown in Fig. 2(b), is always negligible with respect to the other terms.

The mixed term *c*, shown in Fig. 2(c), exhibits a smooth profile with an angular extension in accordance with the angular extension of the object. Differently from the PA case, in place of a tight peak surrounded by a small base, here a much more round profile is reported showing that the specular effect, although always present, is sharply mitigated. This fact is confirmed by the ration between the maximum of the term *c* and the maximum of the term *a*. This ratio is about 2 times lower in the SA case. Finally, although the image obtained by the sum of the 3 terms is strictly dominated the term *c* always in the SA case (as shown in Fig. 2(d)), such an image, far to be perfect, represents the object shape better than in the PA case.

The reduction of the specular behaviour reported in the SA case, and the consequent improvement of the image profile, can be explained by the virtual doubling of the spatial aperture operated by the SA scheme. In fact, reasoning in the PA case where the insonification is generated from the aperture centre, a larger spatial aperture allows to collect more specular reflections. Consequently, the number of beam signals with a significant echo amplitude increases, as it is not limited any more to those with a steering angle very close to the perpendicular to the object surface.

5 CONCLUSIONS

A general description of the nonlinear effects resulting from the square envelope extraction has been provided, and particular attention has been given to the consequence related to the specular effect of smooth objects.

After fixing a given spatial aperture, the advantages of the synthetic aperture in terms of angular resolution and reduction of the specular effect have been stressed by means of simulations in which the object is assumed as a densely packed set of discrete scatterers.

Although the virtual doubling of the spatial aperture, resulting from the adoption of a synthetic aperture approach, is mathematically correct only in far field or at the focalisation distance, for small objects close to the focalisation distance this virtual doubling can be considered the key reason of the above mentioned advantages.

6 REFERENCES

1. J.L. Sutton, "Underwater Acoustic Imaging," IEEE Proceedings, vol. 67, pp. 554-566, April 1979.
2. B.D. Steinberg, H.M. Subbaram, Microwave Imaging Technique, J. Wiley & Sons, New York, 1991.
3. V. Murino, A. Trucco, "Three-Dimensional Image Generation and Processing in Underwater Acoustic Vision, " The Proceedings of the IEEE, vol. 88, pp. 1903-1946, December 2000.
4. R.O. Nielsen, Sonar Signal Processing, Artech House, Boston, 1991.

5. A. Trucco, V. Murino, "On Nonlinear Effects of Envelope Detection in Beamforming Systems," IEEE Trans. Ultrasonics, Ferroelectrics, and Frequency Control, vol. 44, pp. 948-952, July 1997.
6. A. Macovski, "Ultrasonic Imaging Using Arrays," IEEE Proceedings, vol. 67, pp. 484-495, April 1979.
7. L.J. Ziomek, "Three Necessary Conditions for the Validity of the Fresnel Phase Approximation for the Near-Field Beam Pattern of an Aperture," IEEE Journal of Oceanic Engineering, vol. 18, pp. 73-75, January 1993.
8. B.D. Van Veen, K.M. Buckley, "Beamforming: A Versatile Approach to Spatial Filtering," IEEE ASSP Magazine, vol. 5, pp. 4-24, April 1988.
9. O. George, R. Bahl, "Simulation of Backscattering of High Frequency Sound From Complex Objects and Sand Sea-Bottom," IEEE Jour. Ocean. Engin., vol. 20, pp. 119-130, April 1995.

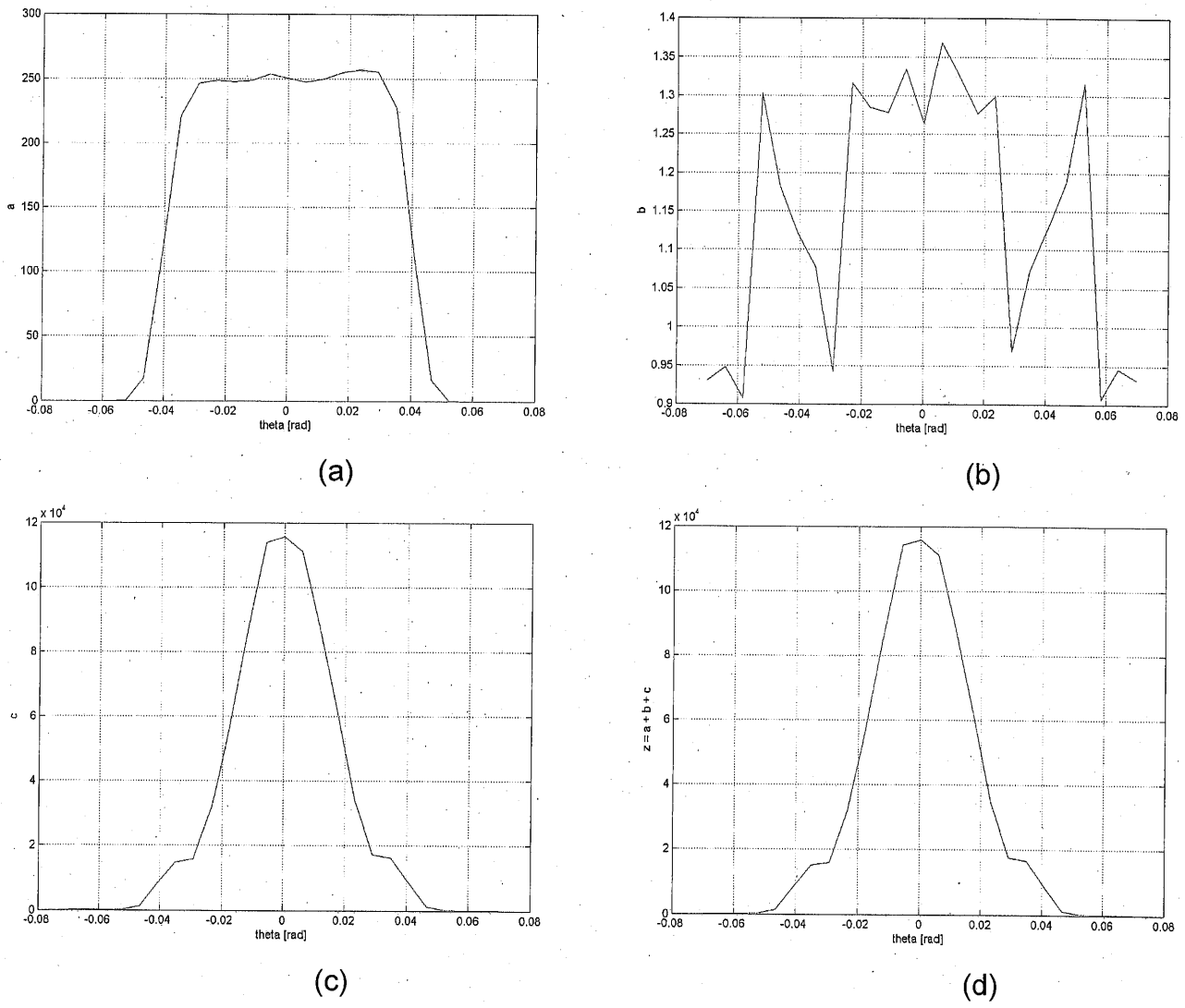

Figure 1. The object response in the PA case, versus the steering angle. (a) the linear term a. (b) the linear term b. (c) the mixed term c. (d) the overall intensity z.

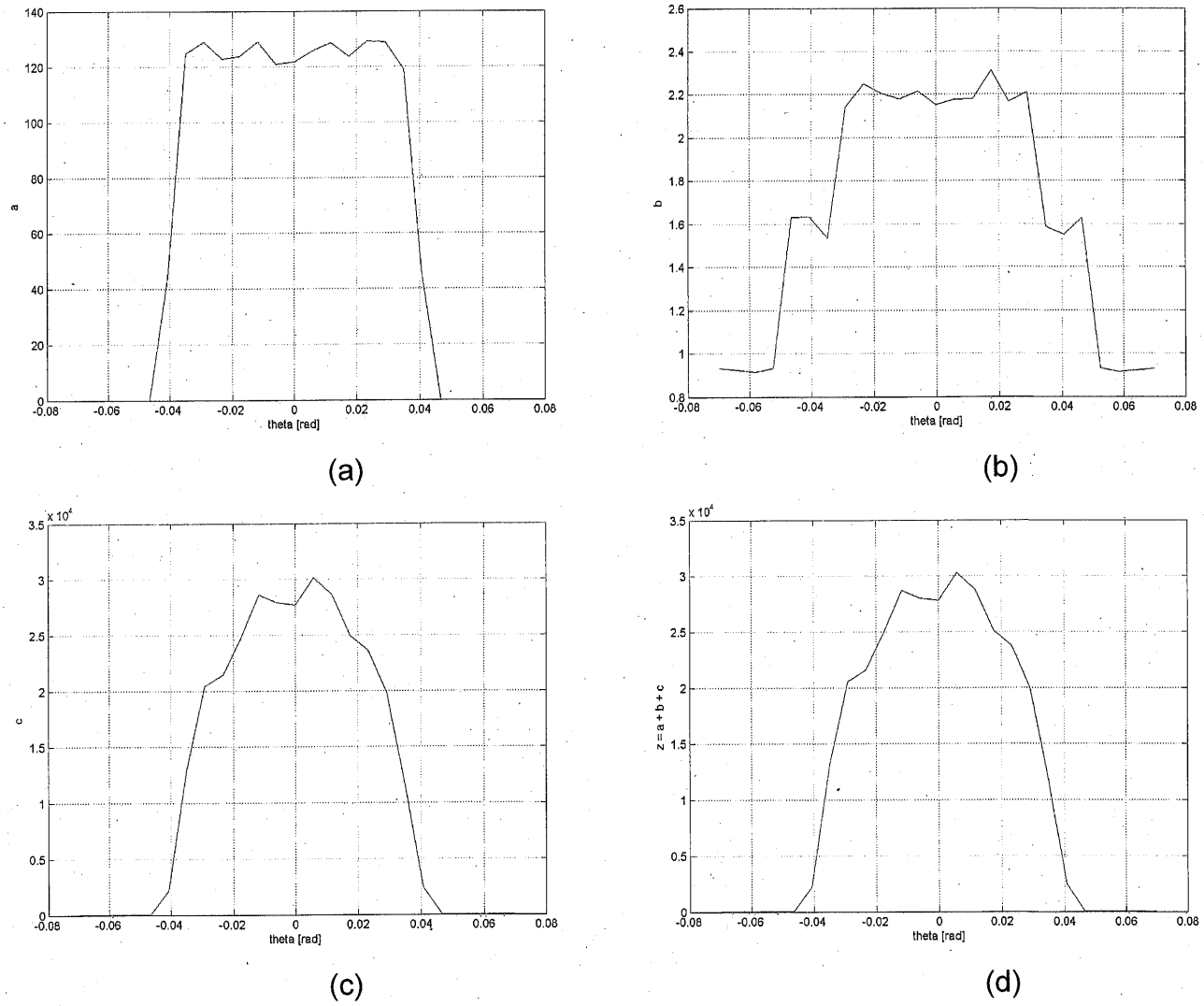

Figure 2. The object response in the SA case, versus the steering angle. (a) the linear term *a*. (b) the linear term *b*. (c) the mixed term *c*. (d) the overall intensity *z*.